# $\mathbb{Z}_2$ Invariance of Germanene on MoS$_2$ from First Principles

Taher Amlaki,[1] Menno Bokdam,[2] and Paul J. Kelly[1]

[1]*Faculty of Science and Technology amd MESA$^+$ Institute for Nanotechnology, University of Twente,*
*P.O. Box 217, 7500 AE Enschede, The Netherlands*
[2]*Faculty of Physics, University of Vienna, Computational Materials Physics, Sensengasse 8/12, 1090 Vienna, Austria*

We present a low energy Hamiltonian generalized to describe how the energy bands of germanene ($\overline{\text{Ge}}$) are modified by interaction with a substrate or a capping layer. The parameters that enter the Hamiltonian are determined from first-principles relativistic calculations for $\overline{\text{Ge}}$|MoS$_2$ bilayers and MoS$_2$|$\overline{\text{Ge}}$|MoS$_2$ trilayers and are used to determine the topological nature of the system. For the lowest energy, buckled germanene structure, the gap depends strongly on how germanene is oriented with respect to the MoS$_2$ layer(s). Topologically nontrivial gaps for bilayers and trilayers can be almost as large as for a freestanding germanene layer.

*Introduction.*—Insulators can be categorized by topological invariants that are not continuous; when these have to change, interesting physics occurs. The first group of these invariants was found to describe the quantum Hall effect for electrons confined in strong magnetic fields [1–3]. A new class of "topological" insulators (TI) was proposed for systems with time-reversal symmetry where the invariant can have two values [4,5] and topologically nontrivial systems are called $\mathbb{Z}_2$ TIs [4–9]. In the two dimensional (2D) graphene ($\overline{\text{C}}$) originally studied by Kane and Mele [4,5], spin-orbit coupling (SOC) leads to the opening of a gap at the Dirac point giving rise to the possibility of topologically protected spin-polarized edge states. The intrinsic SOC of carbon is, however, very small, resulting in gaps of less than 50 $\mu$eV (0.6 K) [10]. Two approaches have been taken to resolve this issue. One is to induce a larger spin-orbit coupling in graphene by placing it in contact with layered materials that contain heavy elements with large intrinsic SOC [11–13]. The other is to begin with a 2D group IV material with a larger intrinsic SOC [14]. Motivated by recent success in growing germanene ($\overline{\text{Ge}}$) on MoS$_2$ [15], this Letter is concerned with the latter.

The structures and stability of freestanding group IV layers have already been studied theoretically. Both silicene ($\overline{\text{Si}}$) and germanene "buckle" with the two sublattices moving in opposite directions out of the original plane but maintaining inversion symmetry [16–18]; stanene ($\overline{\text{Sn}}$) forms a different dumbbell structure [19]. The unsupported layers are predicted to be TIs [19,20]. Experimental efforts have so far focused on growing silicene [21] and germanene [14] on metallic substrates where the intrinsic transport properties cannot be studied. Eventually these layered structures must be transferred to or grown on a nonconducting substrate. It is then essential to know if the TI character survives the interaction with the substrate. However, the complexity of these systems has made

calculation of the topological invariant impossible until now.

We focus on the recently grown $\overline{\text{Ge}}$|MoS$_2$ system [15]. A freestanding, planar germanene layer has a SOC induced gap of 4 meV. Buckling breaks the reflection symmetry, mixes the $p_z$ with the $\{s, p_x, p_y\}$ orbitals and increases the SOC gap to 24 meV [20]. It leads to one Ge sublattice interacting more strongly with a substrate than the other, breaking the sublattice symmetry and opening a gap as large as $\sim$40 meV without SOC; with SOC included, Rashba SOC is induced by the breaking of reflection (and inversion) symmetry. To investigate whether or not the gapped asymmetric bilayer is a TI, we generalize Kane and Mele's model to describe the interaction with a substrate. We use first-principles calculations to determine equilibrium geometries, to evaluate the parameters in the model Hamiltonian from the first-principles electronic structures and to calculate phase diagrams. We will identify the orientation of germanene on the substrate as the most critical factor in determining the size and topological nature of the band gap. The SOC induced band gap of freestanding $\overline{\text{Ge}}$ can be almost completely restored in a MoS$_2$|$\overline{\text{Ge}}$|MoS$_2$ trilayer where the sandwich structure should stabilize and protect the $\overline{\text{Ge}}$ layer from the environment.

*Phenomenological model: asymmetric bilayer.*—We begin by constructing a low energy Hamiltonian for graphene interacting (weakly) with a semiconducting substrate (S) by downfolding a tight-binding (TB) Hamiltonian for the same system. Taking $\boldsymbol{\sigma}$ and $\mathbf{s}$ to be vectors of Pauli matrices where $\boldsymbol{\sigma}$ represents the $A(B)$ sublattices of graphene and $\mathbf{s}$ represents spin, then the result for an asymmetric (AS) $\overline{\text{C}}$|S bilayer is

$$H_{\mathbf{K}}^{\text{AS}}(\mathbf{q}) = \hbar v_F \mathbf{q} \cdot \boldsymbol{\sigma} + \lambda_m \sigma_z + \frac{\lambda_R}{2}(\boldsymbol{\sigma} \times \mathbf{s})_z + \lambda_{\text{so}} \sigma_z s_z + \lambda_B s_z$$

(1)

where $\mathbf{q}$ is the wave vector relative to the $\mathbf{K}$ point, $\mathbf{q} = \mathbf{k} - \mathbf{K}$. $\lambda_m$ is a "mass" term that describes the breaking of the sublattice symmetry by the interaction with the substrate. $\lambda_R$ is a Rashba SOC term that results from the breaking of reflection symmetry in the direction perpendicular to the germanene layer. $\lambda_{so}$ is Kane and Mele's spin-orbit term [4] that contains the intrinsic "atomic" SOC term of monolayer germanene plus $\lambda_{so}^{(ind)}$, the SOC induced by the substrate. $\lambda_B$ corresponds to a "pseudomagnetic" term which is odd under inversion symmetry and changes sign at the $\mathbf{K}'$ point and, therefore, does not break time-reversal symmetry.

The eigenvalues of Eq. (1) at the $\mathbf{K}$ point are

$$\varepsilon_{4(3)} = \lambda_{so} \pm (\lambda_B + \lambda_m), \tag{2a}$$

$$\varepsilon_{2(1)} = -\lambda_{so} \pm \sqrt{(\lambda_B - \lambda_m)^2 + \lambda_R^2}. \tag{2b}$$

By comparing these eigenvalues and the corresponding eigenvectors with those calculated from first principles, we can determine the parameters in Eq. (1) with which the band structure about the Dirac point can be described. The projection of wave functions onto specific atoms is not unique. However, the spin space is complete to very good accuracy and we use the expectation values for the $z$ component of spin

$$\langle s_z \rangle_{n\mathbf{K}} = \frac{1}{\Omega} \int_\Omega \left( |\psi_{n\mathbf{K}}^\uparrow(\mathbf{r})|^2 - |\psi_{n\mathbf{K}}^\downarrow(\mathbf{r})|^2 \right) d^2\mathbf{r} \tag{3}$$

for the four bands at the Dirac point where the integral should be taken over the supercell with area $\Omega$. Applying Eq. (3) to first-principles results to be presented below shows that $\langle s_z \rangle_\mathbf{K} = (s, -s, -1, 1)$ for the four bands at the Dirac point; here $s$ is a positive number smaller than one. Solving for the parameters in Eq. (1) results in

$$\lambda_m = [(\varepsilon_4 - \varepsilon_3) + s(\varepsilon_2 - \varepsilon_1)]/4, \tag{4a}$$

$$\lambda_R = \pm (\varepsilon_2 - \varepsilon_1)\sqrt{1 - s^2}/2, \tag{4b}$$

$$\lambda_{so} = [(\varepsilon_4 + \varepsilon_3) - (\varepsilon_2 + \varepsilon_1)]/4, \tag{4c}$$

$$\lambda_B = [(\varepsilon_4 - \varepsilon_3) - s(\varepsilon_2 - \varepsilon_1)]/4. \tag{4d}$$

When buckling is included, the TB Hamiltonian cannot be exactly downfolded. However, it does not introduce any qualitatively new symmetries and Eq. (1) describes the band dispersion about the Dirac point equally well for planar $\overline{\text{C}}|\text{MoS}_2$ and buckled $\overline{\text{Ge}}|\text{MoS}_2$ as seen in Fig. 1.

*First-principles calculations.*—We use density functional theory (DFT) to calculate ground state energies and optimized geometries with a projector augmented wave (PAW) basis [22,23] as implemented in VASP [24,25] for $\overline{\text{Ge}}|\text{MoS}_2$ bilayers and $\text{MoS}_2|\overline{\text{Ge}}|\text{MoS}_2$ trilayers [26]. We first determine equilibrium geometries for
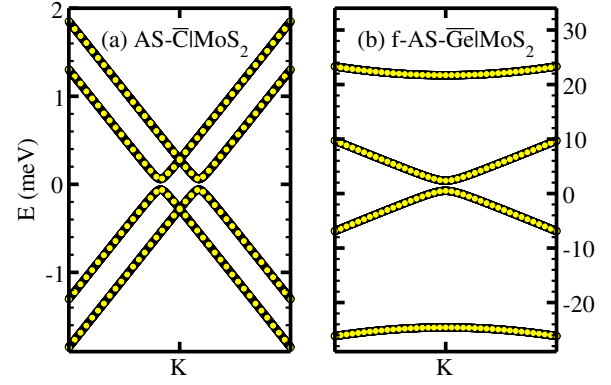


FIG. 1. Band structures of (a) AS $p$-$\overline{\text{C}}|\text{MoS}_2$ and (b) AS $b$-$\overline{\text{Ge}}|\text{MoS}_2$ bilayers close to the $\mathbf{K}$ point. The yellow dots are the results of first-principles calculations, the black lines result from the model (1) with parameters from Eq. (4).

individual monolayers of $\overline{\text{Ge}}$ and $\text{MoS}_2$. For germanene, both planar ($p$-$\overline{\text{Ge}}$) and buckled ($b$-$\overline{\text{Ge}}$) structures are studied. For relaxed $b$-$\overline{\text{Ge}}$ the sublattice planes are separated by $c = 0.71$ Å. The calculated in-plane lattice constants are 4.05, 4.05, and 3.16 Å for $p$-$\overline{\text{Ge}}$, $b$-$\overline{\text{Ge}}$, and $\text{MoS}_2$, respectively. We identify lattice vectors in both materials with an acceptable length mismatch and then rotate the two lattices through an angle $\theta$ to make them coincide; this defines a "supercell."

Because of the weak interaction between germanene and $\text{MoS}_2$, a strong preference for a particular alignment of the two lattices is not expected and this is borne out by the weak binding energy we find for the relaxed structures. We accommodate the small residual lattice mismatch in the $\text{MoS}_2$ layer and reoptimize its structure. The $\overline{\text{Ge}}$ and $\text{MoS}_2$ layers are allowed to bond in two stages, first only changing the height of the $b$-$\overline{\text{Ge}}$ above $\text{MoS}_2$ ($h$-AS structure) and then without constraint ($f$-AS structure). For a supercell, the average buckling is calculated as $c = \sqrt{\sum_{N_{\text{Ge}}} c_i^2 / N_{\text{Ge}}}$ and is given together with other relevant parameters in Table I for the smallest "reasonable sized" supercell containing 89 atoms with $\theta = 24.8°$ and an acceptable lattice mismatch of 0.7%. For the $h$-AS bilayer, the separation of the bottom germanene plane from the upper sulphur layer is 3.11 Å.

*Results: AS bilayers.*—The band structures of $p$-$\overline{\text{C}}|\text{MoS}_2$ and $b$-$\overline{\text{Ge}}|\text{MoS}_2$ bilayers close to the Dirac point are compared in Fig. 1. On this small energy scale, the shape of the bands is quite different because $\lambda_B$ is dominant for graphene while for germanene $\lambda_{so}$, $\lambda_m$, and $\lambda_R$ are much larger. It is clear from the figure that the phenomenological model (black lines) describes the low energy first-principles bands (yellow dots) close to the $\mathbf{K}$ point very accurately for different regimes. For AS $b$-$\overline{\text{Ge}}|\text{MoS}_2$ the gap decreases from 5.6 meV for the height optimized structure ($h$-AS) to 1.9 meV for the fully unconstrained structure ($f$-AS); see Table I. $\lambda_m$ is seen to increase faster than $\lambda_{so}$ because the

TABLE I.   $E_b$ is the binding energy in meV per $\overline{\text{Ge}}$ unit cell. The dimensionless spin parameter $s$ is defined in the text. $\Delta_{\mathbf{K}}$ is the gap calculated at the $\mathbf{K}$ point in meV. The Hamiltonian parameters defined in Eqs. (2) and (4) are given in meV for freestanding planar and buckled $\overline{\text{Ge}}$ layers, for AS $\overline{\text{Ge}}|\text{MoS}_2$ bilayers and for IS $\text{MoS}_2|\overline{\text{Ge}}|\text{MoS}_2$ trilayers. $c$ is the separation between the two Ge planes in Å and $v_F \approx 4 \times 10^5$ $m/s$. For $f$-AS $\overline{\text{C}}$, shown for comparison, the minimum gap is not at $\mathbf{K}$.

| | $E_b$ | $s$ | $\Delta_{\mathbf{K}}$ | $\lambda_m$ | $\lambda_{so}$ | $\lambda_R$ | $\lambda_B$ | $c(\text{Å})$ |
|---|---|---|---|---|---|---|---|---|
| $p$-$\overline{\text{Ge}}$ | | | 4.21 | | 2.11 | | | 0.00 |
| $b$-$\overline{\text{Ge}}$ | | | 25.78 | | 12.89 | | | 0.71 |
| $h$-AS | 328 | 0.83 | 5.55 | 7.95 | 11.60 | 5.72 | −0.56 | 0.71 |
| $f$-AS | 332 | 0.87 | 1.88 | 10.28 | 12.04 | 6.18 | −0.62 | 0.73 |
| $f$-AS ($\overline{\text{C}}$) | 45 | 0.91 | 0.55 | −0.08 | 0.00 | 0.12 | −0.27 | 0.00 |
| $h$-IS | 671 | | 21.21 | | 10.61 | | | 0.71 |
| $f$-IS | 680 | | 22.71 | | 11.36 | | | 0.75 |

average buckling increases slightly from 0.71 to 0.73 Å so the gap decreases. Another important point is that $\lambda_{so}^{(ind)}$ is negative. Calculating $\lambda_{so}^{(ind)} = \lambda_{so}^{h\text{-AS}} - \lambda_{so}^{b\text{-}\overline{\text{Ge}}}$ with parameters from Table I yields $\lambda_{so}^{(ind)} = 11.60 - 12.89 = -1.29$ meV and, therefore, interaction with the $\text{MoS}_2$ layer reduces the intrinsic SOC induced gap of germanene. The mass and Rashba terms are larger than the induced SO term and both $\lambda_m$ and $\lambda_R$ increase faster than $\lambda_{so}^{(ind)}$ if the interaction between germanene and $\text{MoS}_2$ increases. Applying pressure to AS $\overline{\text{Ge}}|\text{MoS}_2$ reduces the gap until $\lambda_{so} = \frac{1}{2}(\lambda_m + \lambda_B + \sqrt{(\lambda_m - \lambda_B)^2 + \lambda_R^2})$ when it vanishes. After that, the band gap grows again but the topological nature of the bands changes. Applying pressure to AS $\overline{\text{Ge}}|\text{MoS}_2$ will therefore not result in a TI with a larger band gap.

To determine the $\mathbb{Z}_2$ topological invariant $\nu$ for the AS system, we analyze the phase space corresponding to Eq. (1) with the parameter values from Table I. $\nu$ is related to the integral of the Berry curvature $B(\mathbf{q})$ over the effective Brillouin zone (EBZ) and the Berry potential over its boundary [36]. In our four band model the full Brillouin zone is $\mathbf{K} \oplus \mathbf{K'}$, the EBZ contains only $\mathbf{K}$ and, therefore,

$$\nu = \left\{ 1 + \frac{1}{2\pi} \int \left[ B_1(\mathbf{q}) + B_2(\mathbf{q}) \right] d\mathbf{q} \right\} \text{mod} \, 2, \quad (5)$$

where $B_i(\mathbf{q})$ is the Berry curvature of the $i$th band and unity in the large parentheses is the contribution of the boundary. Since it is a topological invariant, $\nu$ will not change unless the band gap vanishes so the TI and NI regions should be separated by zero-gap lines. According to Ref. [5], the system will be a TI if the $\lambda_{so}$ term is dominant, whereas if $\lambda_m$ is dominant, the system will be a NI. Any point in the phase space that can be connected to any of the $\lambda_{so}$ dominated points without closing the gap is TI.
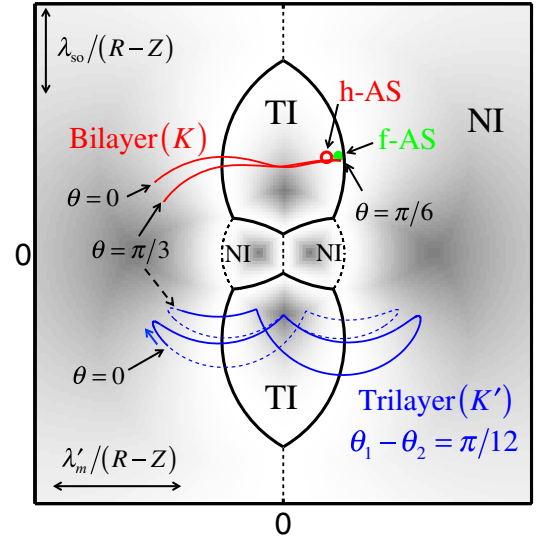


FIG. 2.   Stereographic projection of the phase space of the Hamiltonian (1). Black lines represent boundaries between regions where the gap vanishes; phases on either side of the dashed black lines are the same. The scaling of the $\lambda_{so}$ and $\lambda_m$ variables with $R$-$Z$ is explained in the text. When germanene is rotated with respect to $\text{MoS}_2$, a trajectory is traced out in parameter space which is shown in red for a $\overline{\text{Ge}}|\text{MoS}_2$ bilayer and in blue for a $\text{MoS}_2|\overline{\text{Ge}}|\text{MoS}_2$ trilayer, where the two $\text{MoS}_2$ layers are rotated with respect to one another by $\theta_1 - \theta_2 = 15°$.

The general phase space for the Hamiltonian (1) is four dimensional. Scaling all the parameters will result in scaling of all the eigenvalues so we only need to study the surface of a sphere ($S^3$) of radius $R$ ($R^2 = \text{tr} H^2/4$) in this four dimensional space. Since there are only three independent eigenvalues, we construct a map $\phi: S^3 \to S^2$, where $X \equiv \lambda_m' = (\lambda_m + \lambda_B)/\sqrt{2}$, $Y = \lambda_{so}$, $Z = \sqrt{[\lambda_R^2 + (\lambda_m - \lambda_B)^2]/2}$ and $X^2 + Y^2 + Z^2 = R^2$. Adding a term $-Z$ to symmetrize $\phi$, the eigenvalues at $\mathbf{K}$ will be $\varepsilon_{4(3)} = Y \pm \sqrt{2}X$ and $\varepsilon_{2(1)} = -Y \pm \sqrt{2}Z$. The final step is a conformal map (stereographic projection) $\text{sp}: S^2 \to \mathbb{R}^2$ which results in Fig. 2 [$\text{sp}(\phi): S^3 \to \mathbb{R}^2$]. As long as $|\lambda_B| \leq \sqrt{\lambda_m^2 + \lambda_{so}^2}$—our first-principles calculations will show that this condition is satisfied—the gap remains at the $\mathbf{K}$ point and will be given by this map. The figure shows that for $\theta = 24.8°$ (open red dot), AS $b$-$\overline{\text{Ge}}|\text{MoS}_2$ is a topological insulator—just. Relaxing the germanene layer fully on $\text{MoS}_2$ does not change the $\mathbb{Z}_2$ invariant though the reduced gap means that it is less stable (green dot).

For planar germanene (or graphene [37]), the $\lambda$ parameters depend only weakly on the orientation with respect to the $\text{MoS}_2$ substrate [26]. Buckling brings one germanene sublattice into closer contact with the substrate than the other and this leads to a nonvanishing mass term $\lambda_m$. When germanene is displaced parallel to the substrate, $\lambda_m$ varies very weakly [26] but when it is rotated through some angle $\theta$ it varies strongly as shown in Fig. 3 (red dots and curve).
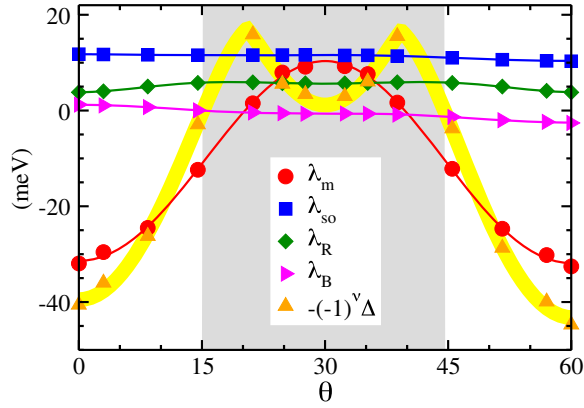
FIG. 3.    $\lambda$ parameters as a function of the angle $\theta$ for a fixed height of germanene above $MoS_2$ that minimizes the energy for $\theta = 24.8°$ for $b$-$\overline{Ge}|MoS_2$. The dashed lines are fits to expressions with appropriate angle symmetries. Details of the calculations and the parameters extracted for both planar and buckled $\overline{Ge}|MoS_2$ can be found in Ref. [26].

This gives rise to a much more complex dependence of the gap on the germanene orientation, $\Delta_K(\theta)$ (yellow triangles and curve). The angle dependence of the other parameters is seen to be much smaller. The shaded part of Fig. 3 is TI and for AS $b$-$\overline{Ge}|MoS_2$ bilayers a sizable gap of more than 15 meV is predicted for angles $\theta \sim 20°$ and $\theta \sim 40°$. In the phase diagram Fig. 2, the full angle dependence is shown as a red line.

$MoS_2|\overline{Ge}|MoS_2$ *trilayers.*—In an experiment it will be necessary to protect the germanene layer. A second, capping layer of $MoS_2$ will most likely be at some arbitrary angle $\theta_2$ to germanene, itself at an angle $\theta_1$ to the substrate $MoS_2$ layer, making it important to know how the gap will depend on $\theta_1$ and $\theta_2$. The large separation of the two $MoS_2$ layers suggests that the direct interaction can be neglected
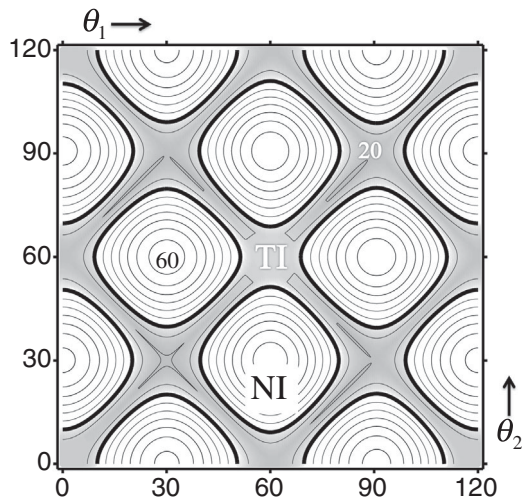


FIG. 4.    Dependence of the band gap on the angles $\theta_1$ and $\theta_2$ that a germanene layer makes with two $MoS_2$ layers in a $MoS_2|\overline{Ge}|MoS_2$ trilayer with threefold rotation symmetry. The unshaded region is NI, the shaded region TI.

in our TB derivation, leading to the prediction that the effect of the two $MoS_2$ layers will be additive in terms of the parameters in Eq. (1). This is confirmed by explicit calculation for trilayers with $(\theta_1, \theta_2) = (24.8°, 24.8°)$, $(24.8°, 3.0°)$, and $(3.0°, 3.0°)$ [26]. The band gap is shown as a function of $\theta_1$ and $\theta_2$ in Fig. 4. The NI gap can be in excess of 60 meV when the $\lambda_m$ contributions do not cancel. The TI gap is largest ($> 20$ meV) when they cancel exactly for $\theta_1 \pm \theta_2 = n\pi/3$ for integer $n$.

*Inversion symmetric trilayer.*—The term containing $\lambda_R$ in Eq. (1) is odd under inversion. For a $MoS_2|\overline{Ge}|MoS_2$ trilayer constructed to have inversion symmetry (IS), the average of $\lambda_R$ over a supercell is zero so this term is absent. The mass term $\lambda_m$ and pseudomagnetic term $\lambda_B$ also vanish because they are odd under inversion and Eq. (1) simplifies to $H_K^{IS}(\mathbf{q}) = \hbar v_F \mathbf{q} \cdot \boldsymbol{\sigma} + \lambda_{so}\sigma_z s_z$. This equation satisfies the requirement of Kramers degeneracy that all bands should be doubly degenerate and predicts that the gap will vanish only if $\lambda_{so}$ is zero. In this case $\langle s_z \rangle$ is not uniquely defined because degenerate bands have complementary spin textures.

Using the effective Hamiltonian parameters calculated for the AS $b$-$\overline{Ge}|MoS_2$ bilayer with $\theta = 24.8°$, we can estimate the band gaps at the $\mathbf{K}$ point for the IS $MoS_2|\overline{Ge}|MoS_2$ trilayer. For the $h$-AS system $\lambda_{so}^{(ind)}$ was found to be $-1.29$ meV. For the $h$-IS configuration, we predict $\lambda_{so}^{(IS)} = \lambda_{so}^{(Ge)} + 2\lambda_{so}^{(ind)} = 12.89 - 2 \times 1.29 = 10.31$. An explicit first-principles calculation yields a value of $\lambda_{so}^{(IS)} = 10.61$ meV. The close agreement between the predicted and calculated values indicates that the model is consistent [26].

For IS systems we can use the formula given by Fu and Kane [7] to determine the TI $\nu$ explicitly from first principles calculations,

$$(-1)^\nu = \prod_{i=1}^{4} \prod_{m=1}^{N} \xi_{2m}(\Gamma_i), \qquad (6)$$

where the first multiplication is over all the time-reversal fixed points $\Gamma_i$ and the second multiplication is over bands with even band number at the $\Gamma_i$; $\xi_{2m}$ is the parity eigenvalue of bands $2m-1$ and $2m$. For our inversion symmetric systems, we explicitly calculated the $\mathbb{Z}_2$ invariant and found them all to be topological insulators with band gaps of about 23 meV generated by SO interactions confirming the phase space assignments.

*Conclusion.*—We use a comprehensive phenomenological model to describe spin-orbit interactions for $\overline{Ge}|MoS_2$ bilayers and $MoS_2|\overline{Ge}|MoS_2$ trilayers. We determine the parameters entering this model from the eigenvalues and spin expectation values at the $\mathbf{K}$ point. The model describes the low energy band structure of germanene very accurately and provides insight into the different interactions involved. For a $\overline{Ge}|MoS_2$ bilayer the band gap of germanene is dominated by the mass term $\lambda_m$ that depends strongly on how germanene is oriented on the $MoS_2$ substrate. A

maximum nontrivial TI gap of ~15 meV is predicted for angles of 20° and 40°. By sandwiching $\overline{Ge}$ between $MoS_2$ layers, the large 24 (26) meV intrinsic SOC gap reported [20] (we find) for freestanding germanene can be almost fully recovered, but requires being able to control the orientation of germanene with respect to both $MoS_2$ layers. Exploratory many-body corrections [26] to these single particle gaps indicate that they may be enhanced by an order of magnitude, making room temperature observation possible.

[1] Y. Zhang, Y.-W. Tan, H. L. Stormer, and P. Kim, Experimental observation of the quantum Hall effect and Berry's phase in graphene, Nature (London) **438**, 201 (2005).

[2] K. I. Bolotin, K. J. Sikes, Z. Jiang, M. Klima, G. Fudenberg, J. Hone, P. Kim, and H. L. Stormer, Ultrahigh electron mobility in suspended graphene, Solid State Commun. **146**, 351 (2008).

[3] M. Z. Hasan and C. L. Kane, Colloquium: Topological insulators, Rev. Mod. Phys. **82**, 3045 (2010).

[4] C. L. Kane and E. J. Mele, $Z_2$ Topological Order and the Quantum Spin Hall Effect, Phys. Rev. Lett. **95**, 146802 (2005).

[5] C. L. Kane and E. J. Mele, Quantum Spin Hall Effect in Graphene, Phys. Rev. Lett. **95**, 226801 (2005).

[6] Liang Fu, C. L. Kane, and E. J. Mele, Topological Insulators in Three Dimensions, Phys. Rev. Lett. **98**, 106803 (2007).

[7] Liang Fu and C. L. Kane, Topological insulators with inversion symmetry, Phys. Rev. B **76**, 045302 (2007).

[8] B. Andrei Bernevig, T. L. Hughes, and S.-C. Zhang, Quantum spin Hall effect and topological phase transition in HgTe quantum wells, Science **314**, 1757 (2006).

[9] M. König, S. Wiedmann, C. Brüne, A. Roth, H. Buhmann, L. W. Molenkamp, X.-L. Qi, and S.-C. Zhang, Quantum spin Hall insulator state in HgTe quantum wells, Science **318**, 766 (2007).

[10] H. Min, J. E. Hill, N. A. Sinitsyn, B. R. Sahu, L. Kleinman, and A. H. MacDonald, Intrinsic and Rashba spin-orbit interactions in graphene sheets, Phys. Rev. B **74**, 165310 (2006); D. Huertas-Hernando, F. Guinea, and A. Brataas, Spin-orbit coupling in curved graphene, fullerenes, nanotubes, and nanotube caps, Phys. Rev. B **74**, 155426 (2006); Y. Yao, F. Ye, X.-L. Qi, S.-C. Zhang, and Z. Fang, Spin-orbit gap of graphene: First-principles calculations, Phys. Rev. B **75**, 041401 (2007); J. C. Boettger and S. B. Trickey, First-principles calculation of the spin-orbit splitting in graphene, Phys. Rev. B **75**, 121402 (2007); M. Gmitra, S. Konschuh, C. Ertler, C. Ambrosch-Draxl, and J. Fabian, Band-structure topologies of graphene: Spin-orbit coupling effects from first principles, Phys. Rev. B **80**, 235431 (2009).

[11] L. Kou, B. Yan, F. Hu, S.-C. Wu, T. O. Wehling, C. Felser, C. Chen, and T. Frauenheim, Graphene-based topological insulator with an intrinsic bulk band gap above room temperature, Nano Lett. **13**, 6251 (2013); T. P. Kaloni, L. Kou, T. Frauenheim, and U. Schwingenschlögl, Quantum spin Hall states in graphene interacting with $WS_2$ or $WSe_2$, Appl. Phys. Lett. **105**, 233112 (2014); L. Kou, S.-C. Wu, C. Felser, T. Frauenheim, C. Chen, and B. Yan, Robust 2D topological insulators in van der Waals heterostructures, ACS Nano **8**, 10448 (2014); L. Kou, F. Hu, B. Yan, T. O. Wehling, C. Felser, T. Frauenheim, and C. Chen, Proximity enhanced quantum spin Hall state in graphene, Carbon **87**, 418 (2015); L. Kou, Y. Ma, B. Yan, X. Tan, C. Chen, and S. C. Smith, Encapsulated Silicene: A robust large-gap topological insulator, ACS Appl. Mater. Interfaces **7**, 19226 (2015).

[12] Z. Wang, D.-K. Ki, H. Chen, H. Berger, A. H. MacDonald, and A. F. Morpurgo, Strong interface-induced spin-orbit interaction in graphene on $WS_2$, Nat. Commun. **6**, 8339 (2015).

[13] M. Gmitra and J. Fabian, Graphene on transition-metal dichalcogenides: A platform for proximity spin-orbit physics and optospintronics, Phys. Rev. B **92**, 155403 (2015).

[14] For recent reviews with additional references, see S. Balendhran, S. Walia, H. Nili, S. Sriram, and M. Bhaskaran, Elemental analogues of graphene: Silicene, germanene, stanene, and phosphorene, Small **11**, 640 (2015); A. Acun, L. Zhang, P. Bampoulis, M. Farmanbar, A. van Houselt, A. N. Rudenko, M. Lingenfelder, G. Brocks, B. Poelsema, M. I. Katsnelson, and H. J. W. Zandvliet, Germanene: The germanium analogue of graphene, J. Phys. Condens. Matter **27**, 443002 (2015).

[15] L. Zhang, P. Bampoulis, A. N. Rudenko, Q. Yao, A. van Houselt, B. Poelsema, M. I. Katsnelson, and H. J. W. Zandvliet, preceding Letter, Structural and Electronic Properties of Germanene on $MoS_2$, Phys. Rev. Lett. **116**, 256804 (2016).

[16] K. Takeda and K. Shiraishi, Theoretical possibility of stage corrugation in Si and Ge analogs of graphite, Phys. Rev. B **50**, 14916 (1994).

[17] G. G. Guzmán-Verri and L. C. Lew Yan Voon, Electronic structure of silicon-based nanostructures, Phys. Rev. B **76**, 075131 (2007).

[18] S. Cahangirov, M. Topsakal, E. Aktürk, H. Şahin, and S. Ciraci, Two- and One-Dimensional Honeycomb Structures of Silicon and Germanium, Phys. Rev. Lett. **102**, 236804 (2009).

[19] P. Tang, P. Chen, W. Cao, H. Huang, S. Cahangirov, L. Xian, Y. Xu, S.-C. Zhang, W. Duan, and A. Rubio, Stable two-dimensional dumbbell stanene: A quantum spin Hall insulator, Phys. Rev. B **90**, 121408 (2014).

[20] C.-C. Liu, W. Feng, and Y. Yao, Quantum Spin Hall Effect in Silicene and Two-Dimensional Germanium, Phys. Rev. Lett. **107**, 076802 (2011).

[21] L. C. Lew Yan Voon and G. G. Guzmán-Verri, Is silicene the next graphene?, MRS Bull. **39**, 366 (2014).

[22] P. E. Blöchl, Projector augmented-wave method, Phys. Rev. B **50**, 17953 (1994).

[23] G. Kresse and D. Joubert, From ultrasoft pseudopotentials to the projector augmented-wave method, Phys. Rev. B **59**, 1758 (1999).

[24] G. Kresse and J. Hafner, *Ab initio* molecular-dynamics for liquid-metals, Phys. Rev. B **47**, 558 (1993).

[25] G. Kresse and J. Furthmüller, Efficient iterative schemes for *ab initio* total-energy calculations using a plane-wave basis set, Phys. Rev. B **54**, 11169 (1996).

[26] See Supplemental Material at http://link.aps.org/supplemental/10.1103/PhysRevLett.116.256805 that invokes additional references for computational details as well as the results of calculations for translations and rotations of both planar and buckled germanene on a $MoS_2$ substrate, which includes Refs. [27–35].

[27] J. Neugebauer and M. Scheffler, Adsorbate-substrate and adsorbate-adsorbate interactions of Na and K adlayers on Al (111), Phys. Rev. B **46**, 16067 (1992).

[28] P. E. Blöchl, O. Jepsen, and O. K. Andersen, Improved tetrahedron method for Brillouin-zone integrations, Phys. Rev. B **49**, 16223 (1994).

[29] M. Dion, H. Rydberg, E. Schröder, D. C. Langreth, and B. I. Lundqvist, Van der Waals Density Functional for General Geometries, Phys. Rev. Lett. **92**, 246401 (2004).

[30] T. Thonhauser, V. R. Cooper, S. Li, A. Puzder, P. Hyldgaard, and D. C. Langreth, Van der Waals density functional: Self-consistent potential and the nature of the van der Waals bond, Phys. Rev. B **76**, 125112 (2007).

[31] J. Klimes, D. R. Bowler, and A. Michaelides, Van der Waals density functionals applied to solids, Phys. Rev. B **83**, 195131 (2011).

[32] L. Hedin, New method for calculating the one-particle green's function with application to the electron-gas problem, Phys. Rev. **139**, A796 (1965).

[33] M. S. Hybertsen and S. G. Louie, Electron correlation in semiconductors and insulators: Band gaps and quasiparticle energies, Phys. Rev. B **34**, 5390 (1986).

[34] M. Shishkin and G. Kresse, Implementation and performance of the frequency-dependent GW method within the PAW framework, Phys. Rev. B **74**, 035101 (2006).

[35] N. Berseneva, A. Gulans, A. V. Krasheninnikov, and R. M. Nieminen, Electronic structure of boron nitride sheets doped with carbon from first-principles calculations, Phys. Rev. B **87**, 035404 (2013).

[36] A. M. Essin and J. E. Moore, Topological insulators beyond the Brillouin zone via Chern parity, Phys. Rev. B **76**, 165307 (2007).

[37] T. Amlaki, Ph.D. thesis, University of Twente, Netherlands, 2016, http://doc.utwente.nl/100180/.